Effective Deposition Potential Induced Size-Dependent Orientation Growth of Bi−Sb Alloy Nanowire Arrays

Xincun Dou, Yonggang Zhu, Xiaohu Huang, Liang Li, and Guanghai Li*

Key Laboratory of Materials Physics, Anhui Key Laboratory of Nanomaterials and Nanoechnology Institute of Solid State Physics, Chinese Academy of Sciences, Hefei 230031, People's Republic of China

Received: June 27, 2006; In Final Form: August 27, 2006

The influence of effective deposition potential on the orientation and diameter of $Bi_{1-x}Sb_x$ alloy nanowire arrays by pulsed electrodeposition technique was reported. X-ray diffraction, field-emission scanning electron microscopy, and transmission electron microscopy analysis show that the orientation of the $Bi_{1-x}Sb_x$ nanowires can be turned from the [110] to the [202] direction by increasing the effective deposition potential, and the nanowires fully fill in the pores of the AAM in the lower potential region, while in the higher potential region the nanowires partly fill the pores of the AAM. The origin of those phenomena and the growth mechanism of the nanowire are discussed together with composition analysis.

Introduction

Thermoelectric materials can directly convert heat to electricity and can be run in reverse as quiet refrigeration units.[1] Theoretical study has indicated that one-dimensional (1D) nanomaterials will have more favorable thermoelectric properties than the two-dimensional thin film or quantum well systems, due to further increases in the density of states,[2] and the study of thermoelectric structures based on nanowires has been extensively increased.

$Bi_{1-x}Sb_x$ alloys form substitutional solid solutions, and their band structure changes gradually from Bi to Sb as x increases.[3,4] Thus, $Bi_{1-x}Sb_x$ nanowires constitute a unique 1D system in which the band structure and other related properties can be tailored by combining quantum confinement effects with Sb alloying effects.[5] Calculations of the thermoelectric properties of the $Bi_{1-x}Sb_x$ alloy nanowire system have proved that with the variation of x and/or the diameter of nanowires, a relatively higher value of figure of merit (ZT) could be obtained in $Bi_{1-x}Sb_x$ nanowires with a relatively larger nanowire diameter compared with Bi nanowires, particularly for p-type nanowires.[6] The ZT value depends not only on the composition and diameter of $Bi_{1-x}Sb_x$ alloy nanowire, but the orientation of the nanowires. The fabrication of $Bi_{1-x}Sb_x$ alloy nanowires with controllable composition, diameters, and orientations is thus very significant.

Different methods have been used to fabricate $Bi_{1-x}Sb_x$ nanowire arrays, such as pressure injecting the molten alloys[5,7] and direct current electrochemical deposition from toxic nonaqueous solutions of dimethyl sulfoxide into anodic alumina membranes (AAMs).[8,9] The pulsed electrochemical deposition of $Bi_{1-x}Sb_x$ nanowires into AAMs from nontoxic aqueous solution has been demonstrated in our previous study.[10]

Recent results show that the pulsed electrodeposition technique is a most efficient method for the growth of uniform and continuous nanowires in the AAM,[10−20] which allows better control over the deposition parameters, such as deposition rate and ion concentration at the deposition interface compared with the direct and alternating current deposition. The pulse parameters are easier to adjust when used to grow single metals with a preferential orientation and single crystalline structure, such as Sb,[11] Ni, [17] Bi,[19,20] Au,[21] and Co.[22] While the growth of binary or ternary alloy is different from that of single metal, the diameter, composition, and orientation of alloy nanowires changes substantially, and depends strongly on the deposition parameters, such as the pulsed voltage, the pulsed time and the pore size of the AAM. Different results have been reported about the controlling factor of the diameter of the Bi−Sb alloy nanowire. Martin and co-workers found that the diameters of $Bi_{1-x}Sb_x$ and $Bi_{2-x}Sb_xTe_3$ nanowires are smaller than the pore diameters of AAM and attributed it to the presence of Sb in the nanowires,[9,23] and concluded that it is possible to grow wires with diameters that are smaller than the pore diameter by changing the growth potential.[8] While in our previous study we found that the diameters of $Bi_{1-x}Sb_x$ nanowires can be controllably modulated by the pulsed parameters,[10] based on these results, it is considered that the diameter depends not only on the electrodeposition potential, but also on the pulse parameters as well.

As we know, the effective deposition potential is a very important factor in the pulsed electrodeposition technique and can be expressed as

$$U_{\text{eff}} = T_{\text{on}}/(T_{\text{on}} + T_{\text{off}})U \quad (1)$$

where T_{on} is the pulsed time, T_{off} the delayed time, U pulsed voltage, and $T_{\text{on}}/(T_{\text{on}} + T_{\text{off}})$ the duty time. One can see that the effective deposition potential will change by varying any parameters in this equation. Nevertheless, the study on the influence of the effective deposition potential on the orientation and diameter of alloy nanowires is still rare.

As an extension of our previous study,[10] in this paper, we report the influence of the effective deposition potential on the orientation and diameter of $Bi_{1-x}Sb_x$ alloy nanowire arrays by the pulsed electrodeposition technique.

Experimental Section

The AAM was prepared with a two-step anodization process as described previously.[24−26] After the second anodization, the

* Address correspondence to this author. Fax: +86-551-5591434. E-mail address: ghli@issp.ac.cn.

10.1021/jp064009k CCC: $33.50
Published on Web 10/06/2006

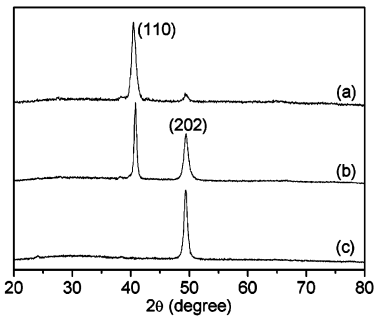

Figure 1. XRD patterns of the $Bi_{1-x}Sb_x$ alloy nanowires deposited at potentials of (a) 0.17, (b) 0.185, and (c) 0.19 V.

AAM was etched by saturated $SnCl_4$ solution to remove the remaining aluminum. The alumina barrier layer was then dissolved in a 5 wt % H_3PO_4 solution at 36 °C for 40 min. The pore size of the AAM is about 60 nm. Finally, a layer of Au film (about 200 nm in thickness) was sputtered on one side of the AAM to serve as the cathode in a two-electrode plating cell, and a graphite plate was used as the counter electrode. The electrolyte for the deposition of $Bi_{1-x}Sb_x$ nanowires contains a mixture of 0.05 M/L $BiCl_3$, 0.02 M/L $SbCl_3$, 50 g/L tartaric acid, 100 g/L glycerol, 70 g/L NaCl, and 1.0 M/L HCl. The pH value of the electrolyte was exactly adjusted to 1.0 by adding appropriate amounts of 5 mol/L aqueous ammonia after 1 day's stability process.

The pulsed electrodeposition was carried out under modulated voltage control from −0.68 to −1.40V with a constant pulsed time T_{on} of 12.5 ms and delayed time T_{off} of 37.5 ms (duty cycle is 25%). From eq 1, one can see the effective deposition potential is from −0.17 to −0.35 V (potential was used and the minus before the potential value is omitted hereafter for simplicity). The deposition temperature is maintained at 18 °C.

Power X-ray diffraction (XRD, Philips PW 1700x with Cu Kα radiation), field-emission scanning electron microscopy (FE-SEM, JEOL JSM-6700F), and transmission electron microscopy (TEM, H-800) were used to study crystalline structures and morphologies of nanowire arrays. The chemical composition of the nanowires was determined by energy dispersive spectrometry (EDS). For XRD measurements, the overfilled nanowires on the surface of the AAM were mechanically polished away. For SEM imaging, the AAM was partly dissolved with 0.5 M NaOH solution and then carefully rinsed with deionized water several times. For TEM observations, the AAM was completely dissolved with 1 M NaOH solution and then rinsed with absolute ethanol.

Results and Discussion

Figure 1 shows typical XRD patterns of the $Bi_{1-x}Sb_x$ alloy nanowires deposited at different potentials. It can be seen that all peaks can be indexed to the Rhombohedral space group $R\bar{3}m$ (to which Bi, Sb, and Bi−Sb alloys belong). The 2θ values of these peaks are between the positions expected for a pure Bi and Sb, indicating the formation of a solid solution. The sharp and narrow peaks indicate that the nanowires have a high preferential orientation. We found that the potential strongly affects the orientation of $Bi_{1-x}Sb_x$ nanowires. When deposited at a potential of 0.17 V, a single strong peak situated at $2\theta = 40.4°$ was found, as shown in curve 1 in Figure 1, which shows a highly preferential orientation along the [110] direction. The same results are obtained at deposition potentials of 0.175 and 0.18 V except for a slight shift of the [110] peak. As the potential increases, the orientation of the nanowires changes, as shown in curve 2 in Figure 1 deposited at a potential of 0.185 V, two orientations have been obtained. As the potential further increased to 0.19 V the orientation of the nanowire changes to the [202] direction, and no changes were found with further increasing potential even to 0.35 V, as shown in curve 3 in Figure 1. These results clearly indicate that the orientation of the $Bi_{1-x}Sb_x$ nanowire strongly depends on the deposition potential, and when the potential is lower than 0.18 V, the nanowires preferentially grow along the [110] direction and when higher than 0.19 V along the [202] direction, and between 0.18 and 0.19 V there is a transition region of the orientation from the [110] to the [202] direction.

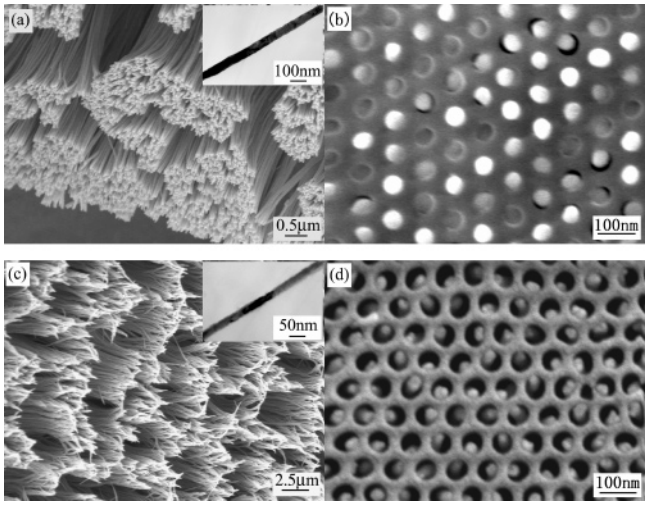

Figure 2. SEM images of $Bi_{1-x}Sb_x$ alloy nanowire arrays with different diameters deposited at potentials of (a and b) 0.18 (nanowire diameter: 60 nm) and (c and d) 0.25 V (nanowire diameter: 28 nm). The insets are the corresponding TEM image of a single nanowire.

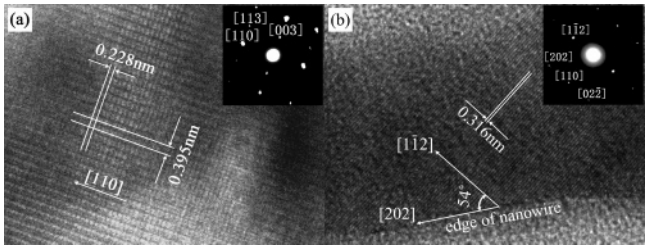

Figure 3. HRTEM image and corresponding SAED pattern of a single $Bi_{1-x}Sb_x$ alloy nanowire deposited at potentials of (a) 0.18 and (b) 0.25 V.

Figure 2 shows the SEM images of the $Bi_{1-x}Sb_x$ alloy nanowire arrays with different diameters deposited at different potentials (the corresponding inset is the TEM image of a single nanowire). When deposited at a potential of 0.18 V, the diameter of the nanowires is about 60 nm, which is equal to the pore size of the AAM, see Figure 2a. The fully filling of the nanowires in the pores of AAM can be seen in Figure 2b (after mechanically polishing away several micrometers of the top surface of the AAM filled with the nanowires by using alumina powders). When deposited at a potential of 0.25 V, the diameter of the alloy nanowires is about 28 nm, see Figure 2c. The partial filling of the nanowires in each pore of the AAM can be clearly seen in Figure 2d, which further proved that the nanowire diameter is smaller than the pore size of the AAM used. It is worth noting that a high filling rate of the nanowires was obtained for all the potentials used.

Figure 3 shows typical HRTEM images and corresponding SAED patterns of the $Bi_{1-x}Sb_x$ alloy nanowires with different diameters at different potentials. The lattice fringes of (003)

TABLE 1: Potential, Composition of Sb in $Bi_{1-x}Sb_x$ Alloy Nanowires, and Nanowire Diameter

potential, V	0.17	0.175	0.18	0.19	0.225	0.25	0.26	0.35
composition of Sb, %	26.7	33.0	30.6	24.5	25.7	23.6	30.0	17.5
nanowire diameter, nm	60	60	60	22	38	28	37	27

and (110) planes with the interplanar distance of about 0.395 and 0.228 nm can be clearly seen in Figure 3a, and the corresponding SAED further confirmed that the alloy nanowires are single crystals and grow along the [110] direction. The clear fringes in Figure 3b correspond to the $(1\bar{1}2)$ plane with the interplanar distance of 0.316 nm, and the angle of about 54° between $[1\bar{1}2]$ and the nanowire axis suggests that the nanowire is along the [202] direction, which are in good agreement with XRD results.

The $Bi_{1-x}Sb_x$ nanowires are deposited on an amorphous Au film that sputtered on the back of the AAM as electrode, which is inert with respect to the growth of the nanowires and has no effect on the nanowire growth.[27] In the initial growth stage of $Bi_{1-x}Sb_x$, the nuclei is random and a newly coalesced compact deposit has a perfectly random orientation;[28] new grains will grow if the size of an initial cluster exceeds the critical dimension N_c.[29] The larger the N_c is, the more favorable it is for a crystal to grow from a previously nucleated seed grain

$$N_c = \frac{8BV_m^2\sigma^3}{27(ze|\eta|)^3} \tag{2}$$

where V_m, σ, z, η, and B are the volume occupied by one atom on the surface of the nucleus, the surface energy, the effective electron number, the deposition potential, and a constant, respectively.[29] Low-surface-energy grains will grow faster than high-energy grains,[30,31] and the rapid growth of low-energy surface at the expense of the high-energy surface results in an increase in grain size, favoring the formation of columnar grain.[28] That is, only the plane whose direction is parallel to the alumina pores can grow up, and it certainly should satisfy the energy minimized principal under the outer conditions.

After the initial nucleation and enlargement of the nucleus, the growth changes to a 2D-like model. The critical dimension N_c for a 2D-like nucleus can be expressed as

$$N_c = bs\epsilon^2/(Ze\eta)^2 \tag{3}$$

where s, ϵ, Z, η, and b are the area occupied by one atom on the surface of the nucleus, the edge energy, the effective electron number, the overpotential, and a constant, respectively.[29] So based on the 2D growth mechanism, the cations move to the surface of the plane that the 3D nuclei mechanism has constructed, are deoxidized, are adhered, and then diffuse. The texture of thicker $Bi_{1-x}Sb_x$ deposits is a result of competitive growth between adjacent grains occurring in a stage of growth after the coalescence stage.[28] So in this process, the nanowires will keep their original growth direction because of the two-dimensional nucleation layer-by-layer growth mode.[32−34] From the above discussion, it can be concluded that the growth of the $Bi_{1-x}Sb_x$ alloy nanowires follows the 3D to 2D model.

Table 1 shows the composition and diameter of the $Bi_{1-x}Sb_x$ alloy nanowires deposited at different potentials in the AAM with the pore size of 60 nm. On the basis of our previous XRD results and this table, we can divide the potential into three regions, i.e., the lower potential region ($\leq$0.18 V), the intermediate potential region (0.18 V $\leq U \leq$ 0.19 V), and the higher potential region ($\geq$0.19 V). It is obvious that the electrocrystalline process depends on the potential, and consequently resulted in the change of the orientation of $Bi_{1-x}Sb_x$ alloy nanowires from [110] to [202] when the potential changes from the lower to the higher region. In the lower potential region, the nanowires fully fill in the pores of the AAM, and in the higher potential region the diameters of nanowires are smaller than the pore size of the AAM. FESEM and TEM observations indicate that the nanowire diameters of $Bi_{1-x}Sb_x$ alloy nanowires deposited in the intermediate potential region have the same feature as those in the higher potential region. The confinement of the nanopore structure in the AAM facilitates the formation of columnar grains and single-crystalline nanowires in the nanopores.[28] It was found that the growth rate of the nanowires is low at the lower potential region, and thus the reduced ions have enough time to transversely diffuse and fully fill the pores, implying that the T_{on} used in this study can fully satisfy the deposition of $Bi_{1-x}Sb_x$ in the pores of the AAM and T_{off} is large enough for the recovery of the ions concentration on the front of the grown nanowires. In the higher potential region, the growth rate of the nanowires is relatively high, the reduced ions do not have enough time to transversely diffuse, and furthermore, the delayed time T_{off} is not large enough to recover the ions consumption on the front of the grown nanowires until a new equilibrium between the reduction and recovery of ions was established, and thus nanowires with a smaller diameter were formed.

From Table 1, one also can see that there is the following tendency: the higher the Sb content, the larger the diameter of $Bi_{1-x}Sb_x$ nanowires in the higher potential region. This result is considered due to the competitive relationship between the uncomplexed Bi^{3+} and Sb^{3+} ions, and their chloride complexes ions at different potentials, resulting in a different Sb content deposited at different potentials. The exact value of the standard potentials of the uncomplexed Bi^{3+} and Sb^{3+} ions $\varphi^{\Theta}_{M^{3+}/M}$, and that of their chloride complexes $\varphi^{\Theta}_{MCl_n^{3-n}/M}$, where M = Bi or Sb, can be found in our previous study,[10] which showed that the standard potentials for different chloride complexes of both elements are very close, indicating that bismuth and antimony will co-deposit as an alloy. Nevertheless, because there are many different chloride complexes, the sensitivity of each chloride complexe on the potential is different, and thus the total co-deposition rates of Bi and Sb are different, resulting in a different diameter at different deposition potentials.

From the above discussion one can see that the potential also determines the diameter of the alloy nanowires. To further prove this conclusion, we keep the potential at a constant 0.25 V and change other parameters: (1) decrease the pore size of the AAM to 45 nm, (2) increases T_{on} to 25 ms, and (3) decrease T_{on} to 5 ms. In the later two cases the duty cycle is still 25%. The results show that the diameter of the nanowires has almost the same value as that shown in Table 1. So, the diameter of the nanowire depends on the potential rather than the pore size of the AAM. But when we maintained the pulsed voltage at 1.0 V, the pore size of the AAM at 60 nm, and the pulsed time T_{on} at 12.5ms, and changed the delayed time T_{off} to either 12.5 or 87.5 ms, i.e., the potential was changed to 0.5 and 0.125 V, respectively. The results showed that no nanowires were formed at a potential of 0.5 V because the delayed time is too short to recover the ions concentration on front of the growth nanowires despite very high potential. But when T_{off} was increased to 87.5 ms, the nanowires have a preferential orientation along the [110] direction because of a very low potential of 0.125 V, as shown in Figure 4. The TEM observation also confirmed that the diameter of the nanowire is 60 nm, and it has the same value

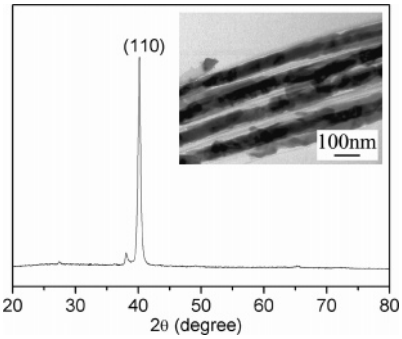

Figure 4. XRD pattern of the $Bi_{1-x}Sb_x$ alloy nanowire arrays deposited at a potential of 0.125 V with T_{on} of 12.5 ms and T_{off} of 87.5 ms. The inset is the corresponding TEM image.

as the pore size of the AAM used, as shown in the inset in Figure 4. Our result indicates that the orientation and diameter of $Bi_{1-x}Sb_x$ alloy nanowires depend on the effective deposition potential, and the proper selection of the pulse parameters is also an important factor in determining the growth of the nanowire. The reduction and recovery rate of uncomplexed Bi^{3+} and Sb^{3+} ions and their chloride complexe ions and the competitive deposition rate of Bi and Sb determined by the effective deposition potential are considered responsible for the transition of nanowire orientation and the change of nanowire diameter.

Our results demonstrate that the orientation and diameter of the $Bi_{1-x}Sb_x$ alloy nanowires with proper composition are controllable through proper selection of the effective deposition potential and pulsed parameters. Rabin's calculations predicted that the n-type $Bi_{1-x}Sb_x$ alloy nanowires with a diameter between 20 and 40 nm and Sb content between 20% to 30% and the p-type $Bi_{1-x}Sb_x$ alloy nanowires with Sb content between 10% to 20% will have better TE properties.[6] Our results show that the n-type $Bi_{1-x}Sb_x$ alloy nanowires with a better TE property can be obtained under the potential of 0.19 to 0.26 V and the p-type $Bi_{1-x}Sb_x$ alloy nanowires under the potential of 0.35 V. The smaller the nanowire diameter is, the stronger the quantum confinement effect is, and thus the n-type $Bi_{1-x}Sb_x$ alloy nanowires, which have a [202] preferential growth orientation and a smaller diameter, should have a relatively higher ZT value than the larger diameter ones which grow preferentially along the [110] direction.

Conclusion

In summary, single-crystalline and highly preferentially oriented $Bi_{1-x}Sb_x$ alloy nanowire arrays have been prepared into porous anodic alumina membrane by pulsed electrodeposition. The growth of the nanowires follows the 3D to 2D mode. It was found that the effective deposition potential controls the orientation and diameter of the $Bi_{1-x}Sb_x$ nanowire. There are two obvious different effective deposition potential regions. In the lower potential region, the nanowires fully fill in the pores of the AAM, and in the higher potential region the nanowires partly fill the pores of the AAM. By increasing the deposition potential from the lower potential region to the higher potential one, the orientation of the $Bi_{1-x}Sb_x$ nanowires can turn from the [110] to the [202] direction. Our results show that through proper selection of the effective deposition potential and pulsed parameters, the orientation and diameter of the $Bi_{1-x}Sb_x$ alloy nanowires can be controllably grown into the AAM, which will favor the fabrication of $Bi_{1-x}Sb_x$-based superlattice nanowires. Further work is underway.

Acknowledgment. This work was supported by the National Natural Science Foundation of China (No. 10474098) and the National Major Project of Fundamental Research for Nanomaterials and Nanostructures (No. 2005CB623603).

References and Notes

(1) Majumdar, A. *Science* **2004**, *303*, 777.
(2) Disalvo, F. J. *Science* **1999**, *285*, 703.
(3) Goldsmid, H. J. *Phys. Status Solidi A* **1970**, *1*, 7.
(4) Lenoir, B.; Dauscher, A.; Devaux, X.; Ravich, Yu. I.; Martin-Lopez, R.; Scherrer, H.; Scherrer. S. In *Proc. IEEE Int. Conf. Thermoelectrics*, *15th* **1996**, 1.
(5) Lin, Y. M.; Cronin, S. B.; Rabin, O.; Ying, J. Y.; Dresselhaus. M. S. *Appl. Phys. Lett.* **2001**, *79*, 677.
(6) Rabin, O.; Lin, Y. M.; Dresselhaus. M. S. *Appl. Phys. Lett.* **2001**, *79*, 81.
(7) Lin, Y. M.; Cronin, S. B.; Rabin, O.; Heremans, J.; Dresselhaus, M. S.; Ying, J. Y. *Mater. Res. Soc. Symp. Proc.* **2001**, *635*, C4301.
(8) Prieto, A. L.; Martín-González, M.; Keyani, J.; Gronsky, R.; Sands, T.; Stacy, A. M. *J. Am. Chem. Soc.* **2003**, *125*, 2388.
(9) Martín-González, M.; Prieto, A. L.; Knox, M. S.; Gronsky, R.; Sands, T.; Stacy, A. M. *Chem. Mater.* **2003**, *15*, 1676.
(10) Li, L.; Li, G. H.; Zhang, Y.; Yang, Y. W.; Zhang, L. D. *J. Phys. Chem. B* **2004**, *108*, 19380.
(11) Zhang, Y.; Li, G. H.; Wu, Y. C.; Zhang, B.; Song, W. H.; Zhang, L. D. *Adv. Mater.* **2002**, *14*, 1227.
(12) Li, L.; Yang, Y. W.; Huang, X. H.; Li, G. H.; Ang, R.; Zhang, L. D. *Appl. Phys. Lett.* **2006**, *88*, 103119-3.
(13) Li, L.; Yang, Y. W.; Huang, X. H.; Li, G. H.; Zhang, L. D. *Nanotechnology* **2006**, *17*, 1706.
(14) Li, L.; Zhang, Y.; Yang, Y. W.; Huang, X. H.; Li, G. H.; Zhang, L. D. *Appl. Phys. Lett.* **2005**, *87*, 031912.
(15) Li, L.; Yang, Y. W.; Huang, X. H.; Li, G. H.; Zhang, L. D. *J. Phys. Chem. B* **2005**, *109*, 12394.
(16) Zhang, Y.; Li, L.; Li, G. H.; Wu, Y. C.; Sheng, Z. G.; Zhang, L. D. *Phys. Rev. B* **2006**, *73*, 113403.
(17) Nielsch, K.; Müller, F.; Li, A. P.; Gösele, U. *Adv. Mater.* **2000**, *12*, 582.
(18) Guo, Y. G.; Wan, L. J.; Zhu, C. F.; Yang, D. L.; Chen, D. M.; Bai, C. L. *Chem. Mater.* **2003**, *15*, 664.
(19) Li, L.; Zhang, Y.; Li, G. H.; Zhang, L. D. *Chem. Phys. Lett.* **2003**, *378*, 244.
(20) Li, L.; Zhang, Y.; Li, G. H.; Wang, X. W.; Zhang, L. D. *Mater. Lett.* **2005**, *59*, 1223.
(21) Liu, J.; Duan, J. L.; Toimil-Molares, M. E.; Karim, S.; Cornelius, T. W.; Dobrev, D.; Yao, H. J.; Sun, Y. M.; Hou, M. D.; Mo, D.; Wang, Z. G.; Neumann, R. *Nanotechnology* **2006**, *17*, 1922.
(22) Ursache, A.; Goldbach, J. T.; Russell, T. P.; Tuominen, M. T. *J. Appl. Phys.* **2005**, *97*, 10J322.
(23) Martín-González, M.; Prieto, A. L.; Gronsky, R.; Sands, T.; Stacy, A. M. *Adv. Mater.* **2003**, *15*, 1003.
(24) Masuda, H.; Fukuda, K. *Science* **1995**, *268*, 1466.
(25) Sander, M. S.; Gronsky, R.; Sands, T.; Stacy, A. M. *Chem. Mater.* **2003**, *15*, 335.
(26) Prieto, A. L.; Sander, M. S.; Martín-González, M.; Gronsky, R.; Sands, T.; Stacy, A. M. *J. Am. Chem. Soc.* **2001**, *123*, 7160.
(27) Amblart, J.; Froment, M.; Maurin, G.; Spyrellis, N.; Trevisan-Souteyrand, E. T. *Electrochim. Acta* **1983**, *28*, 909.
(28) Pan, H.; Liu, B. H.; Yi, J. B.; Poh, C.; Lim, S. H.; Ding, J.; Feng, Y. P.; Huan, C. H. A.; Lin, J. Y. *J. Phys. Chem. B* **2005**, *109*, 3094.
(29) Budevski, E.; Staikov, G.; Lorenz, W. J. *Electrochemical Phase Formation and Growth*: *An introduction to the initial stage of metal deposition*; VCH: New York, 1996; p 267.
(30) Paunovic, M.; Schleinger, M. *Fundamentals of Electrochemical Deposition*; John Wiley & Sons: New York, 1998; p 125.
(31) Srolovitz, D. J.; Mazor, A.; Bukiet, G. G. *J. Vac. Sci. Technol. A* **1988**, *6*, 2371.
(32) Moller, F. A.; Kintrup, J.; Lachenwitzer, A.; Magnussen, O. M.; Behm, R. J. *Phys. Rev. B* **1997**, *56*, 12506.
(33) Lachenwitzer, A.; Magnussen, O. M. *J. Phys. Chem. B* **2000**, *104*, 7424.
(34) Wang, X. W.; Fei, G.; Tao.; Xu, X. J.; Jin, Z.; Zhang. L. D. *J. Phys. Chem. B* **2005**, *109*, 24326.